ROYAL SOCIETY OF CHEMISTRY

PAPER
Luis M. Martínez-Prieto, Avelino Corma *et al.*
Controlling the selectivity of bimetallic platinum–ruthenium nanoparticles supported on N-doped graphene by adjusting their metal composition

Check for updates

Controlling the selectivity of bimetallic platinum–ruthenium nanoparticles supported on N-doped graphene by adjusting their metal composition†

Christian Cerezo-Navarrete, [iD] Yannick Mathieu, [iD] Marta Puche, Cristina Morales,
Patricia Concepción, Luis M. Martínez-Prieto [iD] * and Avelino Corma [iD] *

Mono and bimetallic platinum–ruthenium nanoparticles have been generated on N-doped graphene (NH_2-rGO) following an organometallic approach. Surface and structural studies confirmed the formation of bimetallic MNPs with controlled metal compositions. To evaluate the activity/selectivity of the different materials prepared we used the hydrogenation of acetophenone as a model reaction. We found that both the activity and selectivity of the supported-bimetallic NPs are highly dependent on the support and the atomic composition. The higher the Pt/Ru ratio, the higher the selectivity towards 1-phenylethanol. Indeed, a remarkable activity and selectivity in the hydrogenation of acetophenone was observed for $Pt_5Ru_1@NH_2$-rGO. The reactivity of these catalysts was also investigated in the hydrogenation of other substrates such as functionalized arenes (*i.e.* nitrobenzene and benzaldehyde) or hydroxymethylfurfural (HMF), demonstrating that it is possible to control the activity and selectivity of bimetallic Pt–Ru MNPs supported on N-doped graphene by adjusting their metal composition.

Introduction

Supported transition metal catalysts are of great importance for the industrial synthesis of numerous chemicals.[1,2] These industrial catalysts are usually based on metals well-dispersed on supports, leading to large metal surface area materials with good interaction between the metal and the support that result in active and stable catalysts. Depending on the nature of the metal active sites required, *i.e.* single metal atoms, small metal nanoclusters or metal nanoparticles (MNPs), an appropriate catalyst synthesis method that maximizes the surface population of the desired metal site is necessary.[3] The final activity and selectivity of the metal sites will depend not only on the specific electronic properties of the metal but also on their modifications by the support that can act as a "ligand",[4] specially in the case of single atoms and subnanometric metal clusters. Therefore, the selection of a support with suitable characteristics (high surface area, functionalization with heteroatoms, basic/acid sites, *etc.*) is a key parameter for metal stabilization and its catalytic behaviour. In this context, functionalized materials with two-dimensional (2D) nanolayered structures such as N-doped

graphenes, are attractive supports for MNPs. The presence of functional groups with donor atoms such as nitrogen groups introduces new active sites that alter the local environment of the metallic nanoparticle and facilitates the synergic interaction between MNPs and the support. The doping of graphene improves the catalytic performance of supported MNPs in many catalytic reactions, including hydrogenation,[5] oxidation[6] and coupling reactions,[7] among others. For example, in a recent study we observed that the basic centres of N-doped reduced graphene oxide (NH_2-rGO) next to the active metal sites heterolytically activate H_2, enhancing the activity and selectivity of ruthenium nanoparticles in the selective hydrogenation of fatty acids to alcohols.[8] There is another way to modify the electronic and geometric characteristics of a given metal cluster or nanoparticle that involves the formation of bimetallic entities where the catalytic properties can be modified,[9] controlling the final effect on what occurs in metal materials.[10] Here we have combined both effects by generating bimetallic PtRu NPs over N-doped reduced graphene oxide ($PtRu/NH_2$-rGO), looking for the formation of catalysts that present catalytic properties beyond those of Pt and Ru working separately, together with MNPs with neighbouring basic sites that are able to activate H_2 in a heterolytic way.

Another efficient strategy to modulate the reactivity of MNPs is the use of surface molecules (ligands or metal complexes), which can modify the metal surface–substrate interactions during catalysis and thus change the MNP

ITQ, Instituto de Tecnología Química, Universitat Politècnica de València (UPV),
Av. de los Naranjos S/N 46022, Valencia, Spain.
E-mail: luismiguel.martinez@csic.es, acorma@itq.upv.es

† Electronic supplementary information (ESI) available. See DOI: 10.1039/d0cy02379e

494 | *Catal. Sci. Technol.*, 2021, **11**, 494–505

This journal is © The Royal Society of Chemistry 2021

activity/selectivity. The employment of ligands to decorate/stabilize MNPs and control their surface chemistry is well known in colloidal catalysis,[11] but much less used in supported-MNP catalysis, since it is normally assumed that surface ligands partially block the metal active sites and reduce the catalytic activity of the catalysts, which, in principle, is a non-desired effect.[12] In the same way, molecular complexes, *i.e.* organometallic tin compounds such as tetrabutyltin hydride, have been employed to modify MNP surfaces, and thus improve the activity and selectivity of the nanocatalysts.[13] However, this increase in selectivity is sometimes accompanied by a decrease in activity, since these organotin species somewhat poison the surface nanoparticle obstructing a considerable number of available active sites.[13a] On the other hand, bimetallic nanoparticles present new catalytic properties (*i.e.* selectivity), in comparison to the inherent properties of monometallic NPs, without an evident loss of activity. Even in certain cases, an increase in activity has been observed due to a synergistic effect.[14] For example, the incorporation of a more electropositive metal such as iron, tin or ruthenium in Pt NPs increases their selectivity towards the hydrogenation of carbonyl groups in unsaturated aldehydes/ketones. The presence of a second metal, which acts as an electron donor "ligand", increases the electron density on platinum, and led to the electrophilic activation of the C=O bond.[15]

Herein, we present a series of mono and bimetallic platinum–ruthenium nanoparticles on N-doped graphene, which were obtained by decomposition of the corresponding organometallic precursors, [Pt(NBE)$_3$] (NBE: norbornene) and/or [Ru(COD)(COT)] (COD: cyclooctadiene and COT: cyclooctatriene), under H$_2$ in the presence of the graphene material. To obtain extra anchoring points for MNP stabilization, and to introduce basic centres next to the active metal sites for heterolytic H$_2$ cleavage, N-doped reduced graphene oxide (NH$_2$-rGO) was used as a support. The obtained catalytic systems (Pt/NH$_2$-rGO, Pt$_5$Ru$_1$/NH$_2$-rGO, Pt$_1$-Ru$_1$/NH$_2$-rGO, Pt$_1$Ru$_5$/NH$_2$-rGO and Ru/NH$_2$-rGO) have been characterized from the electronic and geometric points of view, and it has been possible to modulate the catalytic activity and selectivity for the hydrogenation of several substrates with different functional groups by means of the supported bimetallic nanoparticles.

Results and discussion

Synthesis, characterization and surface studies

A series of mono and bimetallic PtRu NPs were generated on N-doped reduced graphene oxide (NH$_2$-rGO) by decomposition of the corresponding organometallic precursors under 3 bar H$_2$ pressure in THF at room temperature (r.t) (Scheme 1). Monometallic Pt/NH$_2$-rGO and Ru/NH$_2$-rGO were prepared following a previously described synthetic method,[8] using Pt(NBE)$_3$ and Ru(COD)(COT), respectively. Bimetallic systems with different metal compositions were obtained after the co-decomposition of Pt(NBE)$_3$ and Ru(COD)(COT) in 5:1, 1:1 and 1:5 molar ratios (Pt$_5$Ru$_1$/NH$_2$-rGO, Pt$_1$Ru$_1$/NH$_2$-rGO and Pt$_1$Ru$_5$/NH$_2$-rGO). These metal precursors were used due to their fast and similar decomposition rates under H$_2$, which lead to the formation of Pt–Ru alloys.[16] The metal contents of the supported NPs (3 wt%) were determined by inductively-coupled plasma (ICP) and X-ray fluorescence analyses (XRF). In all cases, the metal contents and molar ratios are close to the theoretical ones (see Tables S1 and S3, ESI†).

Transmission electron microscopy (TEM) analysis for the mono and bimetallic NPs on NH$_2$-rGO revealed ultrafine, monodispersed and a narrow distribution of NPs within the 1.2–2.5 nm range, with a mean diameter between 1.5 and 2.1 nm (Fig. 1a–e). In particular, Ru NPs supported on NH$_2$-rGO (Ru/NH$_2$-rGO) present the smallest particles with a mean size of 1.5 ± 0.2 nm, whereas the platinum counterpart, Pt/NH$_2$-rGO, exhibit the largest size (2.1 ± 0.4 nm). Bimetallic NPs show intermediate sizes, and the size increases as the percentage of Pt in the system increases (Pt$_1$Ru$_5$/NH$_2$-rGO: 1.6 ± 0.4 nm, Pt$_1$Ru$_1$/NH$_2$-rGO: 1.7 ± 0.3 nm and Pt$_5$Ru$_1$/NH$_2$-rGO: 1.9 ± 0.3 nm) (Fig. 1a–e). According to the results, it is apparently possible to obtain smaller and less agglomerated NPs when the N-doped reduced graphene oxide is used as a support (*i.e.* Pt$_1$Ru$_5$/NH$_2$-rGO: 1.9 ± 0.3 nm – see Fig. 1d) instead of the non-doped analogous reduced graphene oxide (*i.e.* Pt$_1$Ru$_5$/rGO: 2.5 ± 0.5 nm – see Fig. 1f). This phenomenon is very likely due to the fact that N atoms facilitate the interaction between the organometallic precursors and the graphene material during the synthesis, and thus form very small and better-distributed MNPs.[8] In addition, the N atoms present in the graphene act as
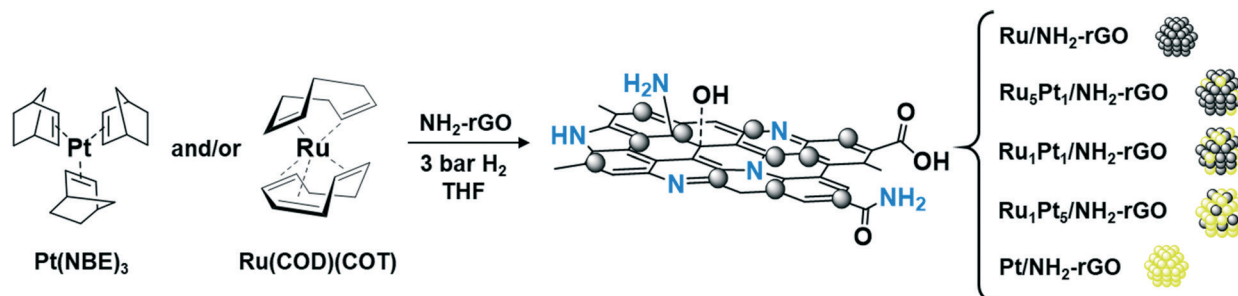
Scheme 1 Generation of mono and bimetallic Pt–Ru nanoparticles on NH$_2$-rGO following the organometallic approach.
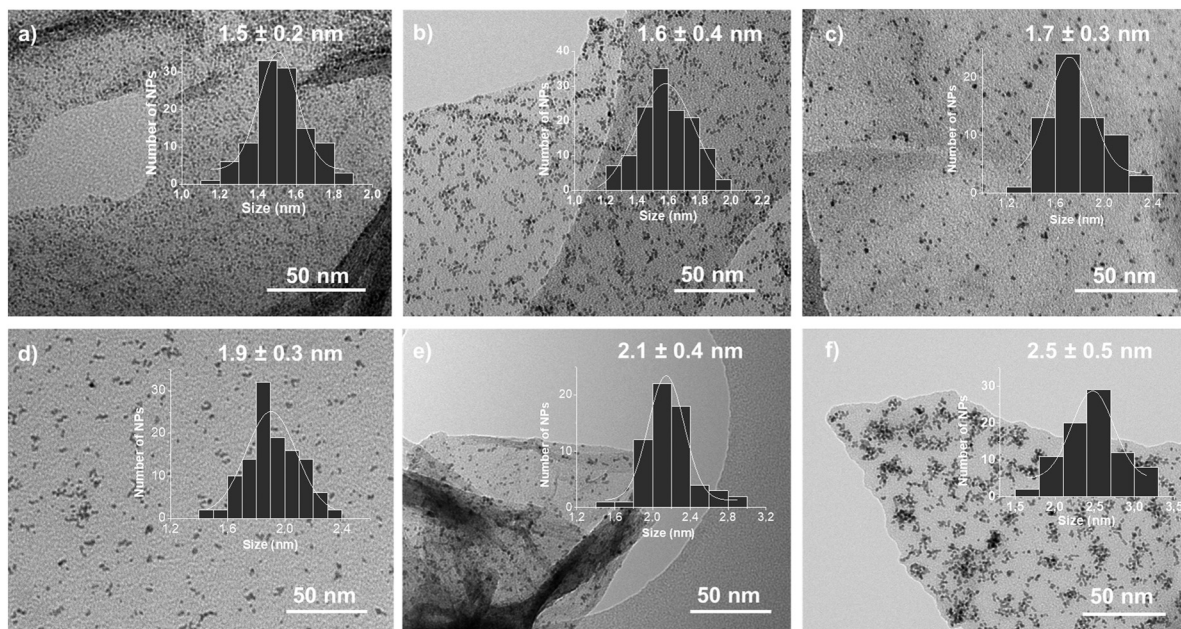
This journal is © The Royal Society of Chemistry 2021

Catal. Sci. Technol., 2021, **11**, 494–505 | **495**

Fig. 1 TEM micrographs and the corresponding size histograms of (a) Ru/NH$_2$-rGO, (b) Pt$_1$Ru$_5$/NH$_2$-rGO, (c) Pt$_1$Ru$_1$/NH$_2$-rGO, (d) Pt$_5$Ru$_1$/NH$_2$-rGO, (e) Pt/NH$_2$-rGO and (f) Pt$_5$Ru$_1$/rGO.

anchoring points for MNPs, increasing their stability and avoiding the agglomeration during catalysis (see hereafter).

High-resolution TEM (HRTEM) analyses confirmed the crystallinity of both mono and bimetallic supported-NPs (Fig. S1, ESI†). Ru in the Ru/NH$_2$-rGO catalyst presents the expected hexagonal close packed (hcp) crystal structure of bulk ruthenium, exhibiting reflections due to the (002), (101) and (002) atomic planes after Fourier analysis (Fig. S1a, ESI†). On the other hand, the HRTEM micrograph of Pt/NH$_2$-rGO shows highly crystalline NPs with a face centered cubic (fcc) structure, typical for bulk Pt. Fourier analysis applied to this image displays reflection planes at (220), (111), (111) and (111) (Fig. S1e, ESI†). Likewise, a fcc crystalline structure is observed for the bimetallic systems, Pt$_1$Ru$_1$/NH$_2$-rGO and Pt$_5$Ru$_1$/NH$_2$-rGO, with inter-planar distances of 2.23 Å and 2.28 Å, respectively, corresponding to the (111) plane in both cases (Fig. S1c and d, ESI†). However, Pt$_1$Ru$_5$/NH$_2$-rGO retains the hcp structure typical of bulk Ru with an inter-planar distance of 2.36 Å that corresponds to the (100) plane (Fig. S1b, ESI†). A similar atomic-packing trend has been previously observed for non-supported Ru–Pt bimetallic NPs with different metal compositions.[17] High-angle annular dark-field scanning electron microscopy coupled with energy-dispersive X-ray spectroscopy (HAADF-SEM EDX) of the bimetallic systems confirmed the presence of alloy NPs with a homogeneous distribution of Pt and Ru. The Pt:Ru % atomic ratios observed by SEM-EDX were Pt$_{21}$Ru$_{79}$, Pt$_{48}$Ru$_{52}$ and Pt$_{76}$Ru$_{24}$ and are close to those expected for Pt$_1$Ru$_5$/NH$_2$-rGO, Pt$_1$Ru$_1$/NH$_2$-rGO and Pt$_5$-Ru$_1$/NH$_2$-rGO, respectively (Fig. S2 and Table S3, ESI†). Such results seem to confirm that the similar decomposition rate of the organometallic precursors used during the synthesis led to the formation of Pt–Ru alloy NPs.[16]

Raman spectroscopy is a model technique to characterize graphene materials, thus, both the support NH$_2$-rGO and the mono and bimetallic catalysts were analyzed by this technique. The spectrum of NH$_2$-rGO presents two bands of similar intensity at 1363 cm^{-1} (band D) and 1603 cm^{-1} (band G), together with a broad band around ca. 3000 cm^{-1} (band 2D′), which is typically associated with 1–2 graphene layers (Fig. S3a, ESI†).[18] The high D/G ratio indicates the high percentage of defect sites of this material, which is very convenient for MNP stabilization. The Raman spectra after the incorporation of the MNPs on NH$_2$-rGO did not show any significant difference (Fig. S3b–f†). A small decrease of the D/G ratio was observed, indicating a higher sp^2 domain, due the incorporation of MNPs.[19] However, it was not possible to observe the vibrations due to the interactions of the carbon, oxygen or nitrogen atoms with the metallic nanoparticles (Pt and/or Ru).

XPS analysis confirmed the chemical composition of this N-doped graphene. The C 1s signal of NH$_2$-rGO exhibits a band at 284.6 eV that can be deconvoluted into three peaks (Fig. S4a, ESI†). The central peak at 284.8 eV corresponds to graphitic carbons (sp^2), and the other two peaks are attributed to carbon atoms bound to N or O (287.0 eV) and carboxylic groups (288.8 eV). Likewise, the N 1s region shows a signal at 399.6 eV that can also be deconvoluted into three components: (i) the main peak at 399.8 eV that belongs to –NH$_2$ and –NH groups, (ii) a peak at 398.6 eV, which corresponds to pyridine-like N atoms, and (iii) the last one at 401.2 eV which is characteristic of graphitic nitrogen atoms (Fig. S4b, ESI†). It is noteworthy that amino and pyrrolic nitrogen groups (–NH$_2$ and –NH) are the most abundant species in this N-doped graphene, which in turn act as basic centres.[8,20]

496 | Catal. Sci. Technol., 2021, 11, 494–505

This journal is © The Royal Society of Chemistry 2021

In addition, the metal composition and the oxidation state of the as-synthetized and previously reduced (180 °C under a H_2 flow for 5 h) supported metal nanoparticles were studied by XPS analysis of the Ru 3p and Pt 4f regions. Fig. S5 (left-hand side, ESI†) shows the Ru $3p_{3/2}$ area of the different as-synthetized catalytic systems with Ru (Ru/NH$_2$-rGO, Pt$_1$Ru$_5$/NH$_2$-rGO, Pt$_1$Ru$_1$/NH$_2$-rGO and Pt$_5$-Ru$_1$/NH$_2$-rGO), where a peak with a binding energy (BE) at *ca.* 463 eV can be observed. The deconvolution of this band presents two different contributions, one at *ca.* 464 eV corresponding to more oxidized species, which can be attributed to Ru(IV) from the RuO$_2$ layer formed after exposure to air, and another one at *ca.* 462 eV (corresponding to more reduced species) characteristic of Ru(0).[21] Indeed, Fig. S5 (right-hand side, ESI†) shows the XPS spectra of Ru $3p_{3/2}$ after reduction and it can be clearly observed that the Ru(0) component at ~462 eV increases at the expense of the RuO$_2$ one. Similarly, Fig. S6 (ESI†) shows the Pt 4f region before (left-hand side) and after reduction (right-hand side) of Pt/NH$_2$-rGO, Pt$_1$Ru$_5$/NH$_2$-rGO, Pt$_1$Ru$_1$/NH$_2$-rGO and Pt$_5$Ru$_1$/NH$_2$-rGO. In this 4f area, we observe the characteristic asymmetric peaks for platinum metal corresponding to the Pt $4f_{7/2}$ and Pt $4f_{5/2}$ signals, with a BE in the range of 70–80 eV. More specifically, in all XPS spectra the Pt $4f_{7/2}$ band is close to *ca.* 72 eV, which can be deconvoluted into two components. One at ~71 eV, characteristic of Pt(0), and another one at *ca.* 73 eV, which is attributed to Pt atoms with a partial positive charge, in part due to the presence of platinum oxides (PtO$_x$) on the MNP surface after air exposure.[22] In the same way as Ru, but in a lower degree, after reduction a fraction of PtO$_x$ is reduced back to Pt(0). The precise Ru(0), RuO$_2$, Pt(0), PtO$_x$ percentages for each sample, before and after reduction, are shown in Table 1. Therefore, it can be concluded that under reduction conditions, very similar to the ones used during the catalytic reactions (*i.e.* 130 °C and 50 bar H_2, see hereafter), supported MNPs are mostly reduced to their respective zero-valent states, which are the active species in hydrogenation reactions, though some oxidized Pt and Ru still exist. Moreover, the surface metal composition of the bimetallic systems was also determined by XPS (Tables S2 and S3, ESI†). All the bimetallic catalytic systems showed an atomic surface composition close to the theoretical ones indicating no surface enrichment with any of the metals forming the bimetallic PtRu NPs.

Catalytic studies

Firstly, the activity and selectivity of the prepared catalysts have been estimated during the hydrogenation of acetophenone (see Table 2 and Fig. 2). Acetophenone has been chosen as a model molecule because it has two potentially hydrogenable functional groups (*i.e.* the ketone and the phenyl groups) and the activity and selectivity of the prepared catalysts can be easily compared. It is important to comment that acetophenone (1) can be reduced to 1-cyclohexylethanol (4) through two distinct hydrogenation routes: (i) route A where the ketone is first hydrogenated to 1-phenylethanol (2) before the complete hydrogenation to form (4) and (ii) route B where the aromatic ring is hydrogenated before the ketone to form 1-cyclohexylethanone (3) (see Table 2, top part).
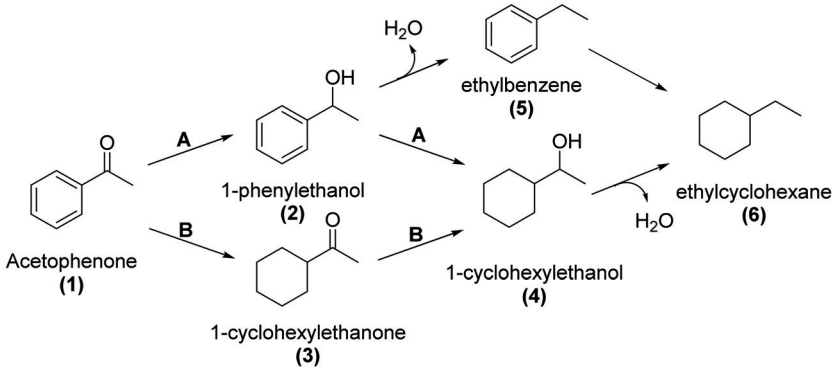
Concerning monometallic catalysts and according to the results, it was found that Pt/NH$_2$-rGO is clearly much less active than Ru/NH$_2$-rGO for the hydrogenation of acetophenone. After 1 hour of reaction, Ru/NH$_2$-rGO presents an estimated conversion of around 92%, whereas the conversion with Pt/NH$_2$-rGO is only 8% (see kinetic data in Fig. 2a and e). The tendency observed at the beginning of the reaction is confirmed at higher reaction time (*i.e.* 20 hours). Almost complete conversion is reached when using the Ru/NH$_2$-rGO catalyst, while a moderate conversion of 63% is obtained with the Pt/NH$_2$-rGO (see Table 2, entries 1 and 5, respectively). With respect to catalyst selectivity, 1-cyclohexylethanol (4) is the main product (*i.e.* ~91% of selectivity after 20 hours of reaction – see Table 2, entry 1) when using Ru/NH$_2$-rGO, and hydrodeoxygenation (HDO) products [*i.e.* ethylbenzene (5) and ethylcyclohexane (6)] are also detected even at short reaction times (see Table 2 entry 1 and Fig. 2a). Meanwhile, the Pt/NH$_2$-rGO catalyst appears to be much more selective to 1-phenylethanol (2) at low (see Fig. 2e) and high conversion rates (*i.e.* >95% after 20 h reaction – see Table 2, entry 5).

On the other hand, bimetallic catalysts present intermediate reactivities between the monometallic Pt and Ru systems. In general terms, the higher the Pt/Ru ratio, the higher the selectivity towards 1-phenylethanol (2), but the lower the activity. After 20 h, Pt$_5$Ru$_1$/NH$_2$-rGO presents a remarkable activity compared to monometallic Pt/NH$_2$-rGO [conversion of 92% with 96% selectivity towards 1-phenylethanol (2)] (Table 2, entry 4). This bimetallic catalyst

Table 1 Oxidation states of Ru/NH$_2$-rGO, Pt/NH$_2$-rGO and Pt$_x$Ru$_y$/NH$_2$-rGO before (left) and after reduction (right) calculated by XPS

Catalyst	Before reduction (%)				After reduction (%)			
	Ru^0	RuO$_2$	Pt^0	PtO$_x$	Ru^0	RuO$_2$	Pt^0	PtO$_x$
Ru/NH$_2$-rGO	41	59	—	—	73	27	—	—
Pt$_1$Ru$_5$/NH$_2$-rGO	34	66	50	50	64	36	67	33
Pt$_1$Ru$_1$/NH$_2$-rGO	36	64	47	53	65	35	60	40
Pt$_5$Ru$_1$/NH$_2$-rGO	31	69	48	52	62	38	66	34
Pt/NH$_2$-rGO	—	—	47	53	—	—	63	37

This journal is © The Royal Society of Chemistry 2021

Catal. Sci. Technol., 2021, **11**, 494–505 | **497**

Table 2 Acetophenone hydrogenation over Ru/NH$_2$-rGO, Pt/NH$_2$-rGO, Pt$_x$Ru$_y$/NH$_2$-rGO, Pt$_5$Ru$_1$/rGO and Ru–Bu$_3$Sn/NH$_2$-rGO^a

Entry	Catalyst	Conversion^{b,c} (%)	Selectivity^b (%)				
			2	3	4	5	6
1	Ru/NH$_2$-rGO	>99	0.0	1.7	90.6	0.1	7.6
2	Pt$_1$Ru$_5$/NH$_2$-rGO	>99	0.7	0.5	92.0	1.3	5.5
3	Pt$_1$Ru$_1$/NH$_2$-rGO	97.2	74.6	1.3	22.5	1.1	0.5
4	Pt$_5$Ru$_1$/NH$_2$-rGO	92.2	96.0	0.3	3.0	0.4	0.3
5	Pt/NH$_2$-rGO	62.9	95.4	0.4	3.5	0.3	0.4
6	Pt$_5$Ru$_1$/rGO	86.9	87.1	3.2	8.3	1.3	0.5
7	Ru–Bu$_3$Sn/NH$_2$-rGO	38.0	97.2	1.4	1.0	0.4	0.0

^{a} Reactions conditions: 0.5 mmol acetophenone, 0.5 mol% cat. (0.0025 mmol metal), 10 mL THF, 50 bar H$_2$, 130 °C, 20 h. ^{b} Conversions and selectivities were determined by GC using dodecane as the internal standard, and confirmed by GC-MS. ^{c} Metal-free NH$_2$-rGO showed negligible activity in the hydrogenation of acetophenone under reaction conditions.
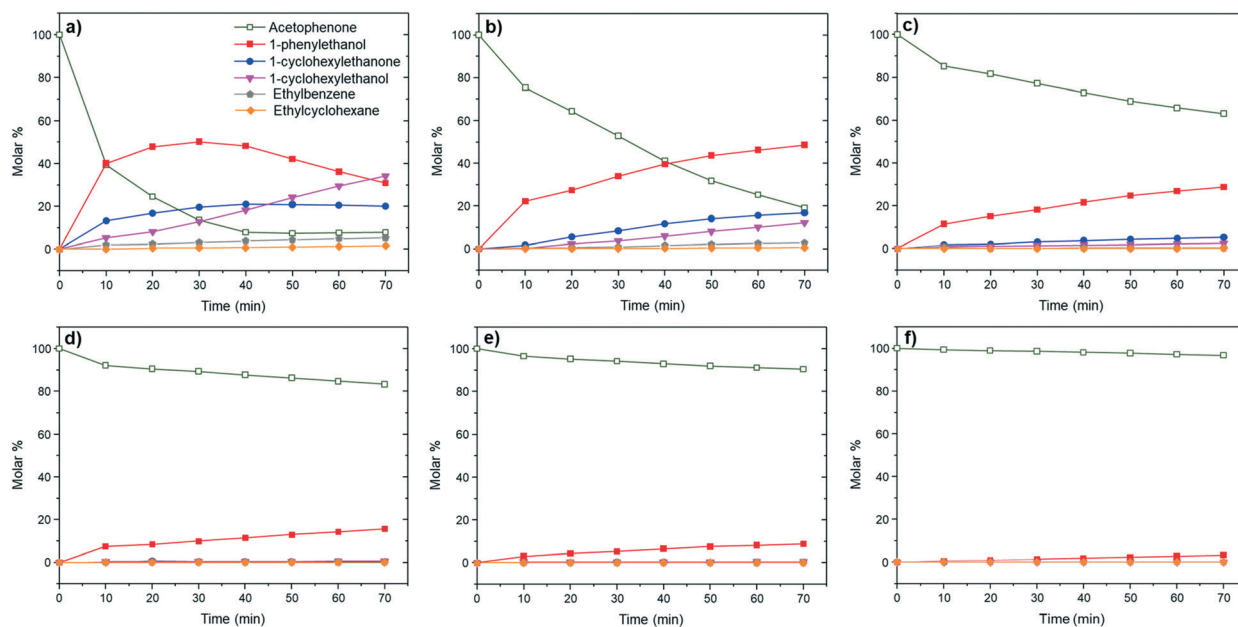

Fig. 2 Hydrogenation of acetophenone using (a) Ru/NH$_2$-rGO, (b) Pt$_1$Ru$_5$/NH$_2$-rGO, (c) Pt$_1$Ru$_1$/NH$_2$-rGO, (d) Pt$_5$Ru$_1$/NH$_2$-rGO, (e) Pt/NH$_2$-rGO and (f) Ru–Bu$_3$Sn/NH$_2$-rGO as catalysts (130 °C, 50 bar H$_2$).

of Pt doped with Ru is as selective as Pt/NH$_2$-rGO in the hydrogenation of acetophenone to 1-phenylethanol (2), but much more active. The presence of a small amount of Ru on the catalyst surface boosts the activity of the supported-Pt NPs, but maintaining the selectivity of Pt/NH$_2$-rGO. The

incorporation of a less electronegative metal (ruthenium) in Pt NPs increases the electron density of Pt, which led to the electrophilic activation of the C=O bond, and increases the activity in the hydrogenation of carbonyl groups.[15] Increasing the Ru content of the catalytic system (i.e. Pt$_1$Ru$_1$/NH$_2$-rGO

498 | Catal. Sci. Technol., 2021, **11**, 494–505

This journal is © The Royal Society of Chemistry 2021

catalyst, with a Ru : Pt molar ratio of 1 : 1), the initial reaction rate is enhanced, however, it is accompanied by a loss in selectivity (see Fig. 2c). Indeed, after 20 h, the conversion is around *ca.* 97% with only *ca.* 75% selectivity to 1-phenylethanol (2) (Table 2, entry 3). This trend was confirmed with Pt$_1$Ru$_5$/NH$_2$-rGO, which presents a higher initial conversion rate but lower selectivity towards 1-phenylethanol (2) (Fig. 2b). After 20 h of reaction time, full conversion is reached for Pt$_1$Ru$_5$/NH$_2$-rGO with a chemoselectivity similar to monometallic Ru/NH$_2$-rGO (Table 2, entries 1 and 2). Altogether, the obtained results clearly indicate that it is possible to control the activity and selectivity of graphene-supported bimetallic Pt–Ru MNPs during the hydrogenation of acetophenone by finely tuning their metal composition.
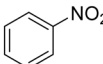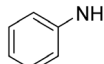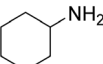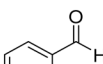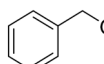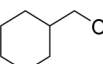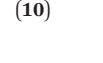
Moreover, it is worth commenting that the formation of benzyl alcohols by the selective hydrogenation of aromatic ketones is normally carried out by homogeneous catalysts.[23] When heterogeneous catalysts are used, a mixture of (2), (3) and (4) is generally obtained.[24] Nevertheless, MNPs immobilized on basic supports have been recently reported as efficient catalysts for selective hydrogenation reactions.[25] Among these catalysts we can find Ru/NH$_2$-rGO, which presents a high selectivity in the hydrogenation of fatty acids,[8] due to the presence of basic sites next to the active metal centres that heterolytically split H$_2$ and enhances the hydrogenation of polar C=O bonds. To confirm this support effect on the new bimetallic catalysts herein presented, we generated Pt$_5$Ru$_1$ MNPs on reduced graphene oxide (rGO). The lack of N-atoms on Pt$_5$Ru$_1$/rGO is reflected in a loss of activity and selectivity compared to Pt$_5$Ru$_1$/NH$_2$-rGO (Table 2, entries 4 and 6). After 20 h, Pt$_5$Ru$_1$/rGO only shows a conversion of 87% with a selectivity to 1-phenylethanol (3) of 87%. Besides, the formation of 3% of 1-cylohexylethanone (4), 8% of 1-cyclohexylethanol (3), and traces of the HDO products (5 and 6) is observed. As the metal composition (see the Experimental part) and MNP size (Fig. 1f) of Pt$_5$Ru$_1$/rGO are in the same range as those of the analogous N-doped catalyst, (*i.e.* Pt$_5$Ru$_1$/NH$_2$-rGO), we can assume that N-doped

graphene enhances the selectivity of the bimetallic catalyst in the hydrogenation of the carbonyl groups in the aromatic ketones. Therefore, the high activity and selectivity observed for Pt$_5$Ru$_1$/NH$_2$-rGO are due to the combination of two factors: (i) the electronic modification of Pt by Ru in the bimetallic nanoparticles that favours their interaction with the carbonyl group and (ii) the cooperative work between the metallic surface and the nitrogen atoms of the support to dissociate H$_2$ heterolytically.

As mentioned in the introduction, another efficient way to control the selectivity of MNPs is through their surface functionalization with organic molecules or molecular complexes.[12,13] However, this surface modification is usually accompanied with a loss of activity. Then, Ru/NH$_2$-rGO was decorated with 0.5 equiv. of tributyltin hydride (Ru–Bu$_3$Sn/NH$_2$-rGO, Fig. S7, ESI†) and tested in the hydrogenation of acetophenone under the standard conditions (20 h at 130 °C and 50 bar H$_2$). The functionalization of Ru/NH$_2$-rGO NPs with this organometallic tin complex increases their selectivity, but considerably decreases their activity (Fig. 2f). Specifically, after 20 h, the conversion is only 38% with a selectivity towards 1-phenylethanol (2) of 97% (Table 2, entry 7). Interestingly, this was not the case for the bimetallic system Pt$_5$Ru$_1$/NH$_2$-rGO, where the activity is much less affected (*i.e.* 96% of 1-phenylethanol at 92% conversion; Table 2, entry 4). Although the use of surface molecules to control the selectivity is an efficient strategy, the characteristic loss of activity makes *a priori* the bimetallic systems more attractive catalysts.

The reactivity of Pt$_5$Ru$_1$/NH$_2$-rGO was compared with the monometallic Pt and Ru catalysts for the hydrogenation of other functionalized arenes such as nitrobenzene or benzaldehyde (Table 3). In general, a similar trend was observed for acetophenone, Ru/NH$_2$-rGO being the most active system but the less selective. For example, in the hydrogenation of nitrobenzene (Table 3, entries 8–10), Ru/NH$_2$-rGO not only allows the complete conversion of the substrate, but also shows the higher reactivity for the over reduced product (55% cyclohexylamine). On the other hand, the bimetallic and

Table 3 Hydrogenation of functionalized arenes over Ru/NH$_2$-rGO, Pt/NH$_2$-rGO and Pt$_5$Ru$_1$/NH$_2$-rGO

Entry/Catalyst	Substrates	Products	Conditions[a]	Conv.[b]	Selectivity[b]
8/Ru/NH$_2$-rGO	NO$_2$ (7)	NH$_2$ (8) + NH$_2$ (9)	H$_2$ (30 bar), 1 h, 100 °C	>99%	**8 : 9** = 45 : 55
9/Pt$_5$Ru$_1$/NH$_2$-rGO				>99%	**8 : 9** = 95 : 5
10/Pt/NH$_2$-rGO				>99%	**8 : 9** = 97 : 3
11/Ru/NH$_2$-rGO	O H (10)	OH (11) + OH (12)	H$_2$ (50 bar), 4 h, 130 °C	>99%	**11 : 12 : 13** = 84 : 9 : 7
12/Pt$_5$Ru$_1$/NH$_2$-rGO		(13)		93%	**11 : 12 : 13** = 100 : 0 : 0
13/Pt/NH$_2$-rGO				67%	**11 : 12 : 13** = 100 : 0 : 0

[a] Reactions conditions: 0.5 mmol substrate, 0.5 mol% cat. (0.0025 mmol metal), 10 mL THF. [b] Conversions and selectivities were determined by GC using dodecane as the internal standard, and confirmed by GC-MS.

platinum systems exhibit a similar reactivity, both being highly selective to aniline at full conversion. When comparing the reactivity of these catalytic systems with benzaldehyde (Table 3, entries 11–13), again the monometallic ruthenium catalyst shows the highest activity but the lowest selectivity. After 4 h, Ru/NH$_2$-rGO presents full conversion and 84% selectivity towards benzyl alcohol, whereas the conversion of benzaldehyde with Pt/NH$_2$-rGO is only 67%, being totally selective to the aromatic alcohol. In between, we could find the activity of Pt$_5$-Ru$_1$/NH$_2$-rGO, which presents great selectivity of platinum but with a much higher activity (100% selectivity towards the aromatic alcohol at 93% conversion).

Owing to the potential activity and selectivity of Pt$_5$/NH$_2$-rGO for hydrogenation reactions, we have also studied here the reduction of an important biomass derived platform molecule such as 5-hydroxymethylfurfural (HMF). The selective hydrogenation of the formyl group to produce 2,5-bis(hydroxymethyl)furan (BHMF) is gaining increasing attention since it is a bio feedstock of high industrial potential.[26] A variety of products can be obtained during the catalytic reduction of HMF, as can be seen in Fig. 3a. The hydrogenation products are mainly BHMF and 2,5-bis(hydroxymethyl)tetrahydrofuran (BHMTHF), depending on whether the aldehyde group is only reduced, or the HMF is totally hydrogenated. Moreover, during the catalysis, HDO products such as 5-methylfurfural (5-MF), 2-hydroxymethyl-5-methylfuran (MFA) or 2-hydroxymethyl-5-methyltetrahydrofuran (MTHFA) can also be formed.

Comparing the results for the different products after 4 h of reaction (Fig. 3b–d), it can be clearly observed that although Ru/NH$_2$-rGO is the most active catalyst (96% conversion), Pt$_5$-Ru$_1$/NH$_2$-rGO shows a similar activity, but with superior selectivity to the desired BHMF (87% of BHMF at 93% conversion). Meanwhile, Ru/NH$_2$-rGO only shows 78% selectivity towards the symmetric diol BHMF, forming also BHMTHF (18%) and MFA (4%). A noticeable amount of the HDO product, MFA, is also observed for Pt$_5$Ru$_1$/NH$_2$-rGO (10%). On the other hand, monometallic Pt/NH$_2$-rGO is clearly the least active system, but the most selective one (94% of BHMF at 83% conversion). Again, we can conclude that the bimetallic system Pt$_5$Ru$_1$/NH$_2$-rGO is almost as active as Ru/NH$_2$-rGO, but maintaining the high selectivity of Pt/NH$_2$-rGO. Doping with Ru the graphene-supported Pt NPs strongly increase the activity of Pt while preserving its high selectivity for the hydrogenation of the carbonyl group.

To investigate the stability and recyclability of Pt$_5$Ru$_1$/NH$_2$-rGO NPs a series of experiments were carried out. First, this bimetallic system was analyzed by TEM and HRTEM after catalysis (*i.e.* hydrogenation of acetophenone). TEM micrographs revealed MNPs with a similar size and metal distribution to the as-synthesized Pt$_5$Ru$_1$/NH$_2$-rGO NPs (2.3 ± 0.7 nm; Fig. S8, ESI†). On the other hand, TEM images of Pt$_5$Ru$_1$/rGO NPs after catalysis showed a significant increase in MNP size (5.8 ± 1.2 nm; Fig. S9, ESI†) and a considerable amount of aggregates. This demonstrates the efficiency of N-doped graphene to stabilize the nanoparticles on the
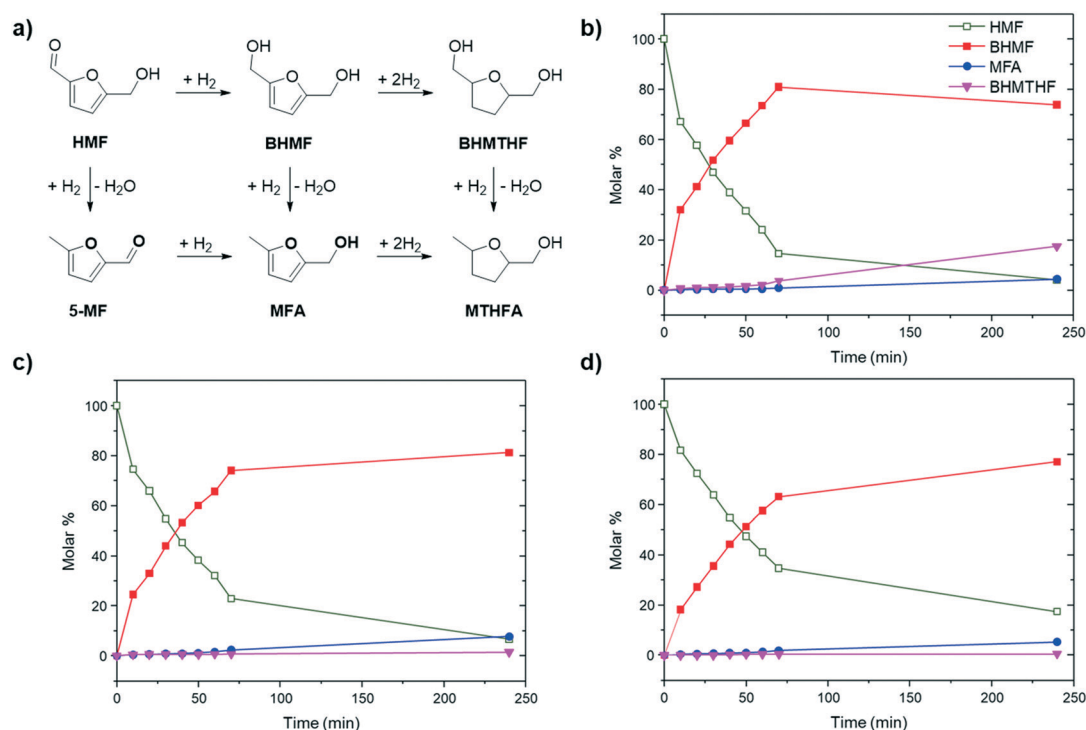

Fig. 3 (a) Catalytic transformation of hydroxymethylfurfural (HMF) using (b) Ru/NH$_2$-rGO, (c) Pt$_5$Ru$_1$/NH$_2$-rGO and (d) Pt/NH$_2$-rGO as catalysts (130 °C, 50 bar H$_2$, in THF). 5-Methylfurfural (5-MF), 2,5-bis(hydroxymethyl)furan (BHMF), 2-hydroxymethyl-5-methylfuran (MFA), 2,5-bis(hydroxymethyl)tetrahydrofuran (BHMTHF), 2-hydroxymethyl-5-methyltetrahydrofuran (MTHFA).
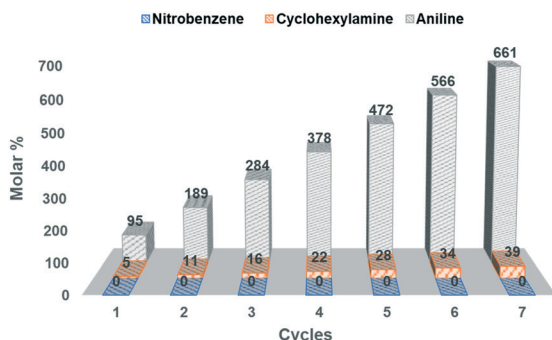
Fig. 4 Multiple addition experiment for the hydrogenation of nitrobenzene catalyzed by Pt_5Ru_1/NH_2-rGO. Conditions: nitrobenzene (0.5 mmol), Pt_5Ru_1/NH_2-rGO NPs (0.5 mol% cat.; 0.0025 mmol metal), THF, 30 bar H_2, 100 °C, 1 h. Every hour, nitrobenzene (0.5 mmol) was added to the reaction mixture. Conversions and selectivities were determined by GC using dodecane as the internal standard, and confirmed by GC-MS.

graphene sheets even under harsh reaction conditions (20 h, 130 °C and 50 bar H_2), preventing their agglomeration. HRTEM analysis confirmed that Pt_5Ru_1/NH_2-rGO NPs after catalysis (Pt_5Ru_1/NH_2-rGO$_{after}$) still maintain their crystalline structure (Fig. S1f, ESI†). In particular, the nanoparticles present an fcc crystalline structure with a lattice spacing of 2.28 Å that corresponds to the (111) plane. To test the recyclability of Pt_5Ru_1/NH_2-rGO, a multiple addition experiment was carried out. More precisely, the hydrogenation of nitrobenzene was performed in a multiple way by using Pt_5Ru_1/NH_2-rGO as a catalyst, and after seven consecutive additions of nitrobenzene, the activity and selectivity of Pt_5Ru_1/NH_2-rGO remain constant (Fig. 4). This result confirms the stability of the catalyst with time under catalytic conditions. TEM analysis of Pt_5Ru_1/NH_2-rGO NPs after the multiple addition experiment showed no significant differences in size, dispersion and distribution (Fig. S10, ESI†), which is in line with the high stability of this catalyst. To prove the heterogeneous nature of Pt_5Ru_1/NH_2-rGO, a "hot filtration" test was carried out during a HMF hydrogenation reaction (130 °C, 50 bar H_2, 10 ml THF). After 50 min of reaction, Pt_5Ru_1/NH_2-rGO was removed by thermal filtration and the reactor was re-charged with the starting feed. After 4 h at 130 °C and 50 bar H_2, no change in the conversion is observed; it remained at 63% (Table S5, ESI†), while almost full conversion is obtained in the presence of the catalyst (Fig. 3c). This result, together with the absence of metal leaching observed by ICP after the "hot filtration" (see the Experimental part), confirms that the reaction is heterogeneously catalyzed.

Experimental

General considerations and starting materials

All chemical operations were carried out using standard Schlenk tubes, Fischer–Porter bottle techniques or in a glove-box under an argon atmosphere. Solvents were purified before use; THF (Sigma-Aldrich) by distillation under an argon atmosphere through filtration in the column of a purification system (MBraun). Ru(COD)(COT) and Pt(NBE)$_3$ were purchased from Nanomeps, and acetophenone (99%), 1-phenylethanol (98%), 1-cyclohexylethanol (97%), ethylbenzene (99%), ethylcyclohexane (99%), hydroxymethylfurfural (99%), benzaldehyde (99%), nitrobenzene (99%) and dodecane (99%) from Sigma Aldrich. All reagents were used without purification, except for HMF which is purified by filtering with an equimolar silica : alumina mixture, and stored in a refrigerator.

Transmission electron microscopy (TEM) and high resolution TEM (HRTEM). All the catalysts were observed by TEM and HRTEM after deposition of a drop of the solution on a copper grid. TEM analyses were performed at the "Servicio de Microscopia Electrónica" of Universitat Politècnica de València (UPV) by using a JEOL JEM 1010 CX-T electron microscope operating at 100 kV with a point resolution of 4.5 Å. The approximation of the particle mean size was made by measuring a number of particles on a given grid. HRTEM observations were carried out with a JEOL JEM 2010 electron microscope working at 200 kV with a resolution point of 2.35 Å. FFT (fast Fourier transform) treatments have been carried out with Digital Micrograph version 3.7.4.

Elemental analysis (EA). EA analyses were performed using a Euro EA3000 elemental analyzer (EuroVector) employing sulfanilamide as a reference.

Inductively coupled plasma (ICP). ICP analyses of Ru/NH$_2$-rGO, Pt$_1$Ru$_5$/NH$_2$-rGO, Pt$_1$Ru$_1$/NH$_2$-rGO, Pt$_5$Ru$_1$/NH$_2$-rGO and Pt$_5$Ru$_1$/rGO were performed by the ICP technique service of the Instituto de Tecnología Química (ITQ), using a Varian 715-ES ICP-optical emission spectrometer. The samples for ICP were prepared following a modified digestion method reported elsewhere.[27] In particular, 30 mg of catalyst samples were suspended in 21 mL of a mixture HCl : HNO$_3$ (6 : 1). The solution was then sonicated for 90 minutes and the samples were digested at 180 °C for 15 hours. After that, it was cooled down until room temperature (r.t.), diluted with 100 mL of water and analyzed by ICP.

X-ray fluorescence analysis (XRF). XRF analyses of Pt$_1$Ru$_5$/NH$_2$-rGO, Pt$_1$Ru$_1$/NH$_2$-rGO, Pt$_5$Ru$_1$/NH$_2$-rGO, Pt/NH$_2$-rGO and Pt$_5$Ru$_1$/rGO were performed using a JASCO FP-8300 equipment. In all cases, the calibration curve was measured using commercially available reactants with different proportions of Pt (Pt@C of 1, 3 and 5%).

Raman. Raman spectra were recorded using an excitation of 514 and 785 nm with a Renishaw inVia Raman spectrometer equipped with a Leica microscope. The samples (powder) were deposited in an Al support, and measured in the region between 0 and 3000 cm^{-1} with a resolution of <4 cm^{-1}.

X-ray photoelectron spectroscopy (XPS). XPS analyses were performed using a SPECS device equipped with a Phoibos 150-9MCD detector using Mg Kα radiation ($h\nu$: 1235.6 eV) and Al Kα radiation ($h\nu$: 1483.6 eV) from a dual source. The pressure during the measurements was kept under 10^{-9} Torr. The quantification and titration of the spectra were performed with the help of the software CASA, referencing

This journal is © The Royal Society of Chemistry 2021

Catal. Sci. Technol., 2021, **11**, 494–505 | **501**

them to C1s = 284.5 eV. The five catalysts were measured before and after reduction (180 °C under a H_2 flow for 5 h).

Gas chromatography (GC). The spectra of the reactants and their hydrogenated products were recorded with an Agilent Technologies 7890A GC-system with a flame ionization detector and an HP-5 column. The method used starts with the injection temperature T_0. After holding this temperature for 2 min, the column is heated to temperature T_1 (10 °C min^{-1}) and finally, the column is heated to T_3 (30 °C min^{-1}) and held for 1 min (T_0 = 80 °C, T_1 = 160 °C, T_2 = 280 °C). On the other hand, HMF and derivative spectra were recorded with a Varian CP-3800 equipment with an automatic injector Varian CP-8400 and a Carbowax column. The method used starts with an injection temperature of 50 °C. After holding the temperature for 1 minute, the column is heated to 240 °C (20 °C min^{-1}) maintaining this temperature for 3.5 minutes. Dodecane has been used as the internal standard.

Gas chromatography coupled to mass spectrometry (GC/MS). GC-MS analyses were carried out using an Agilent 6890N chromatograph equipped with an HP-5 column (30 m, 0.32 mm, 0.25 μm) coupled to an Agilent 5973N electron impact mass spectrometer.

Synthesis of graphenes

NH_2-rGO. NH_2-rGO was obtained following a modified synthetic method previously reported elsewhere:[28] 100 mg of GO (prepared by a modified Hummers method)[29] was dispersed in 40 mL of ethylene glycol with the help of an ultra-sonicator (3 h). After that, 1 mL of ammonia water (25%) was added to the dispersion (dark brown), which was then transferred to a Teflon-lined autoclave and heated at 175 °C for 16 h. Finally, the precipitate was filtered, washed with distilled water until pH = 7, and dried at 60 °C for 24 h. Elemental analysis: N: 7.91%, C: 75.43%, H: 1.69%. XRD: 2θ = 24.2° characteristic of reduced graphene oxide, indicating the reduction of GO to NH_2-rGO. IR: (KBr pellet, cm^{-1}), 1580 cm^{-1} (v N–H) and 1020 cm^{-1} (v C–N).

GO. GO was obtained by a modified Hummers method:[29] Elemental analysis: C: 48.2%, S: 1.6%, H: 2.2%, N: 0.06%. XRD: 2θ = 11.5° assigned to the (001) plane and corresponds to an interlayer separation of d = 7.64 Å. IR: (KBr pellet, cm^{-1}), 3600–2400 cm^{-1} (v stretching O–H), 1700–1733 cm^{-1} (v C=O), 1630–1612 cm^{-1} (v H_2O), 1060 cm^{-1} (v C0), 1384 cm^{-1} (v bending O–H), 1270 cm^{-1} (v O–H phenolic).

rGO. rGO was obtained by thermal reduction/exfoliation at low temperature of GO prepared by a modified Hummers method:[28] GO was introduced into a quartz reactor and then heated at 400 °C for 15 min in a N_2 atmosphere (5 °C min^{-1}). After that, the reactor was cooled down to room temperature in a N_2 atmosphere for 1 : 30 h. Elemental analysis: C: 83.6%, H: 0.5%, S: 0.14%.

Synthesis of monometallic catalysts

Ru/NH_2-rGO. This material has been prepared with the following procedure.[8] A Schlenk flask was charged with Ru(COD)(COT) (10 mg, 0.032 mmol) and dissolved in 3 mL THF. After that, the solution was added to a 100 mL Fischer–Porter bottle charged with a suspension of NH_2-rGO (100 mg) in 50 mL of THF previously sonicated for 90 min. The Fischer–Porter was then pressurized with 3 bar of H_2, and the dispersion was stirred vigorously. The stirring was continued for 20 h at room temperature. After that, the remaining H_2 pressure was released and Ru/NH_2-rGO was separated from the suspension by filtration through a polyamide membrane (Whatman® membrane filters, 47 mm × 0.45 μm) and washed with THF (150 mL). The resulting black precipitate was dried overnight at 60 °C. The size of the NPs was measured by TEM on a sample of at least 100 nanoparticles, which afforded a mean value of 1.5 ± 0.2 nm. ICP gave the following Ru content: 2.5% for Ru/NH_2-rGO.

Pt/NH_2-rGO. The same procedure as previously described for Ru/NH_2-rGO has been followed, with the difference that the organometallic precursor used is Pt(NBE)$_3$ (8 mg, 0.017 mmol). The size of the nanoparticles was measured by TEM, analyzing a sample with at least 100 nanoparticles, obtaining an average value of 2.1 ± 0.4 nm. The metallic content has been quantified by XRF, giving an experimental value of 2.4%.

Synthesis of bimetallic catalysts

Pt$_1$Ru$_5$/NH_2-rGO. A Fischer–Porter bottle was charged with NH_2-rGO (100 mg) and dispersed in 50 mL of anhydrous and deoxygenated THF using ultrasound for 90 minutes. Then, 2 mg of Pt(NBE)$_3$ (0.0042 mmol) and 5 mg of Ru(COD)(COT) (0.016 mmol) were added to the Schlenk flask in a dry box and dissolved in 3 mL of THF. The solution is transferred *via* a cannula to the Fischer–Porter bottle and the resulting mixture was pressurized with 3 bar of H_2. After 20 h under vigorous stirring, the pressure is released and the resulting solid, Pt$_1$Ru$_5$/NH_2-rGO, is filtered under vacuum using a polyamide membrane (Whatman® membrane filters, 47 mm × 0.45 μm) and washed with THF (150 mL). Finally, Pt$_1$Ru$_5$/NH_2-rGO was dried at 60 °C for 24 h. The size of the nanoparticles has been measured by TEM, analyzing a catalyst sample containing at least 100 nanoparticles, which afforded a mean value of 1.6 ± 0.4 nm. The metallic content has been quantified by ICP and XRF, giving an experimental value of 1.7% Ru and 0.7% Pt.

Pt$_1$Ru$_1$/NH_2-rGO. The same procedure as previously described for Pt$_1$Ru$_5$/NH_2-rGO has been followed, with the difference that 5 mg Pt(NBE)$_3$ (0.010 mmol) and 3 mg Ru(COD)(COT) (0.010 mmol) were added. The size of the nanoparticles was measured by TEM, analyzing a sample of the catalyst with at least 100 nanoparticles, obtaining an average value of 1.7 ± 0.3 nm. The metallic content has been quantified by ICP and XRF, giving an experimental value of 0.9% Ru and 1.9% Pt.

Pt$_5$Ru$_1$/NH_2-rGO. The same procedure as previously described for Pt$_1$Ru$_5$/NH_2-rGO has been followed, with the difference that 7 mg Pt(NBE)$_3$ (0.015 mmol) and 1 mg

502 | *Catal. Sci. Technol.*, 2021, **11**, 494–505

This journal is © The Royal Society of Chemistry 2021

Ru(COD)(COT) (0.0032 mmol) were added. The size of the nanoparticles was measured by TEM, analyzing a sample of the catalyst with at least 100 nanoparticles, obtaining an average value of 1.9 ± 0.3 nm. The metallic content has been quantified by ICP and XRF, giving an experimental value of 0.3% Ru and 2.6% Pt.

Pt_5Ru_1/GO. The same procedure as previously described for Pt_5Ru_1/NH_2-rGO has been followed, but we used rGO as a support now. The size of the nanoparticles was measured by TEM, analyzing a sample of the catalyst with at least 100 nanoparticles, obtaining an average value of 2.5 ± 0.5 nm. The metallic content has been quantified by ICP and XRF, giving an experimental value of 0.4% Ru and 2.5% Pt.

Ru–Bu_3Sn/NH_2-rGO. The same procedure as previously described for Ru/NH_2-rGO has been followed, with the difference that 0.5 equivalent of tributyltin hydride was added after the formation of Ru/NH_2-rGO following a similar procedure to that reported elsewhere.[13] The size of the nanoparticles was measured by TEM, analyzing a sample of the catalyst with at least 100 nanoparticles, obtaining an average value of 1.5 ± 0.3 nm. The metallic content has been quantified by ICP, giving an experimental value of 2.6%.

Hydrogenation reactions

The hydrogenation of acetophenone, nitrobenzene, benzaldehyde and hydroxymethylfurfural was carried in a 25 mL engineer autoclave equipped with a mechanical stirrer (750 rpm). Hydrogenations were performed such that the molar ratio metal–substrate was 1 : 200. Thus, taking into account that 0.5 mmol of substrate was used and each catalyst has 3% of the corresponding metal, 0.5 mol% of metal-catalyst was added into each reaction (0.0025 mmol). The exact mass of catalysts added during the catalysis is shown in Table S4 (see the ESI†).

The determined amount of the catalyst in each case was dispersed in 10 mL of THF sonicating for 90 minutes. The mixture was then transferred into the reactor and this one was purged with H_2 three times, and finally charged with 35 bar H_2. The reactor was then heated at 150 °C, reaching a final pressure of 50 bar. The catalyst is kept under these conditions for two hours, to ensure the reduction and activation of the active metal. Before the substrate (0.5 mmol) is introduced with the help of a 250 μL Hamilton syringe, the temperature is reduced to the desired temperature (100 or 130 °C) to carry out the reaction. After holding the reaction for the time required, we stopped the heater and the reactor was left to reach room temperature. Then, the mechanical stirring was stopped and the H_2 pressure removed. Finally, the catalyst was separated by filtration, and the products of the reaction mixture were analyzed by GC using dodecane as the internal standard.

Kinetic experiments

For the kinetic experiments, the autoclave was charged, pressurized and heated under the required conditions and aliquots were taken from the reaction medium and analyzed by GC, using dodecane as the internal standard.

Multiple addition experiment

For the multiple addition experiment, the autoclave was charged, pressurized and heated under the required conditions for nitrobenzene hydrogenation (100 °C, 30 bar H_2, 10 ml THF). Each hour, an aliquot was taken from the reaction medium and a new starting material (*i.e.* nitrobenzene) was added to the reactor. The aliquots were analyzed by GC, using dodecane as the internal standard. The activity and selectivity remained over 7 catalytic cycles confirming the stability of the catalyst.

"Hot filtration" and leaching experiments

For the "hot filtration" experiment, the autoclave was charged, pressurized and heated under the required conditions for HMF hydrogenation (130 °C, 50 bar H_2, 10 ml THF). After 50 min, Pt_5Ru_1/NH_2-rGO was removed by filtration, and the reactor was charged with the mother liquor, pressurized and heated under the same conditions. Then, the conversion of HMF was determined after 4 h and compared to that at 50 min (Table S5, ESI†). No change in the conversion was observed. After thermal filtration, the mother liquor was analysed by ICP and ruthenium and platinum detected were negligible.

Conclusions

Bimetallic PtRu NPs of different metal composition (5 : 1, 1 : 1 and 1 : 5) have been generated on N-doped reduced graphene oxide (NH_2-rGO) by co-decomposition of two organometallic precursors, namely $[Pt(NBE)_3]$ and $[Ru(COD)(COT)]$. The similar decomposition rates of the precursors led to the formation of alloy NPs. These supported-bimetallic NPs, together with their monometallic analogues (Ru/NH_2-rGO and Pt/NH_2-rGO), were fully characterized by TEM, HRTEM, STEM-EDX, Raman and XPS. Different surface metal compositions depending on the Pt/Ru ratio used during the synthesis process were observed for the bimetallic systems. Interestingly, both the activity and selectivity of these PtRu NPs were highly dependent on the nanoparticle composition and the support employed. To evaluate the activity and selectivity of the catalytic systems prepared, the hydrogenation of acetophenone was used as a model reaction. While monometallic Ru/NH_2-rGO NPs showed a high conversion to the over reduced product (1-cyclohexylethanol), Pt/NH_2-rGO exhibited great selectivity towards 1-phenylethanol, but with a much lower activity. In-between we can find the reactivity of supported-bimetallic NPs, Pt_5Ru_1/NH_2-rGO being the most interesting catalyst since it is as selective as Pt/NH_2-rGO but much more active. The remarkable activity and selectivity of Pt_5Ru_1/NH_2-rGO are due to two factors: (i) the electron-density modification of Pt by Ru that activates the C=O bonds and (ii) the cooperative work between the N atoms of graphene and the metal active

sites, which dissociates H_2 in a heterolytic way, and enhances the selectivity towards the hydrogenation of polar bonds, such as carbonyls. The reactivity of this bimetallic catalyst was also investigated in the hydrogenation of other substrates such as functionalized arenes (*i.e.* nitrobenzene and benzaldehyde) or hydroxymethylfurfural (HMF), proving that it is possible to control the activity/selectivity of supported-bimetallic PtRu NPs by tuning their metal surface composition. Finally, the stability and recyclability of Pt_5Ru_1/NH_2-rGO was explored by multiple addition and "hot filtration" experiments, demonstrating to be a stable and recyclable catalyst. The remarkable activity, selectivity and stability of these bimetallic catalytic systems make them interesting candidates for future selective catalysis.

Conflicts of interest

There are no conflicts to declare.

Acknowledgements

Notes and references

1 M. J. Climent, A. Corma and S. Iborra, *Chem. Rev.*, 2011, **111**, 1072.

2 A. Corma and H. Garcia, *Top. Catal.*, 2008, **48**, 8.

3 (*a*) L. Liu and A. Corma, *Chem. Rev.*, 2018, **118**, 4981; (*b*) L. Liu and A. Corma, *Nat. Rev. Mater.*, 2020, DOI: 10.1038/s41578-020-00250-3; (*c*) L. Liu, M. López-Haro, C. W. Lopes, C. Li, P. Concepcion, L. Simonelli, J. J. Calvino and A. Corma, *Nat. Mater.*, 2019, **18**, 866; (*d*) B. Ni and X. Wang, *Adv. Sci.*, 2015, **2**, 1500085; (*e*) M. R. Axet and K. Philippot, *Chem. Rev.*, 2020, **120**, 1085.

4 (*a*) Q.-L. Zhu and Q. Xu, *Chem*, 2016, **1**, 220; (*b*) Y.-Z. Chen, G. Cai, Y. Wang, Q. Xu, S.-H. Yu and H.-L. Jiang, *Green Chem.*, 2016, **18**, 1212; (*c*) A. Noujima, T. Mitsudome, T. Mizugaki, K. Jitsukawa and K. Kaneda, *Angew. Chem., Int. Ed.*, 2011, **50**, 2986.

5 (*a*) L. Xia, D. Li, J. Long, F. Huang, L. Yang, Y. Guo, Z. Jia, J. Xiao and H. Liu, *Carbon*, 2019, **145**, 47; (*b*) S. Pisiewicz, D. Formenti, A.-E. Surkus, M.-M. Pohl, J. Radnik, K. Junge, C. Topf, S. Bachmann, M. Scalone and M. Beller, *ChemCatChem*, 2016, **8**, 129; (*c*) P. Liu, G. Li, W.-T. Chang, M.-Y. Wu, Y.-X. Li and J. Wang, *RSC Adv.*, 2015, **5**, 72785; (*d*) A. Mollar-Cuni, D. Ventura-Espinosa, S. Martín, Á. Mayoral, P. Borja and J. A. Mata, *ACS Omega*, 2018, **3**, 15217.

6 (*a*) S. A. Giles, Y. Yan and D. G. Vlachos, *ACS Catal.*, 2019, **9**, 1129; (*b*) C. S. Ramirez-Barria, M. Isaacs, C. Parlett, K. Wilson, A. Guerrero-Ruiz and I. Rodríguez-Ramos, *Catal. Today*, 2019, **357**, 8; (*c*) X. Xie, J. Long, J. Xu, L. Chen, Y. Wang, Z. Zhang and X. Wang, *RSC Adv.*, 2012, **2**, 12438.

7 (*a*) R. V. Siva Prasanna Sanka, K. Balaji, Y. Leterrier, S. Pandey, M. Srivastava, A. Srivastava, W. H. Binder, S. Rana and V. Michaud, *Chem. Commun.*, 2019, **55**, 6249; (*b*) M. Kuniyil, V. S. J. Kumar, F. S. Adil, R. M. Shaik, M. Khan, E. M. Assal, R. H. M. Siddiqui and A. Al-Warthan, *Catalysts*, 2019, **9**, 469; (*c*) X. Zhao, J. Xie, X. Liu and X. Liu, *Appl. Organomet. Chem.*, 2019, **33**, 4623.

8 L. M. Martínez-Prieto, M. Puche, C. Cerezo-Navarrete and B. Chaudret, *J. Catal.*, 2019, **377**, 429.

9 M. Sankar, N. Dimitratos, P. J. Miedziak, P. P. Wells, C. J. Kiely and G. J. Hutchings, *Chem. Soc. Rev.*, 2012, **41**, 8099.

10 (*a*) F. Gao and D. W. Goodman, *Chem. Soc. Rev.*, 2012, **41**, 8009; (*b*) N. M. Wilson, P. Priyadarshini, S. Kunz and D. W. Flaherty, *J. Catal.*, 2018, **357**, 163.

11 (*a*) L. M. Martínez-Prieto and B. Chaudret, *Acc. Chem. Res.*, 2018, **51**, 376; (*b*) L. M. Martínez-Prieto and P. W. N. M. van Leeuwen, Ligand effects in ruthenium nanoparticle catalysis, in *Recent Advances in Nanoparticle Catalysis*, Springer Science, 2020.

12 S. Kunz, *Top. Catal.*, 2016, **59**, 1671.

13 (*a*) E. Bonnefille, F. Novio, T. Gutmann, R. Poteau, P. Lecante, J.-C. Jumas, K. Philippot and B. Chaudret, *Nanoscale*, 2014, **6**, 9806; (*b*) L. M. Martínez-Prieto, J. Marbaix, J. M. Asensio, C. Cerezo-Navarrete, P.-F. Fazzini, K. Soulantica, B. Chaudret and A. Corma, *ACS Appl. Nano Mater.*, 2020, **3**, 7076.

14 J.-Y. Ruzicka, D. P. Anderson, S. Gaw and V. B. Golovko, *Aust. J. Chem.*, 2012, **65**, 1420.

15 (*a*) P. Claus, *Top. Catal.*, 1998, **5**, 51; (*b*) P. Mäki-Arvela, J. Hájek, T. Salmi and D. Y. Murzin, *Appl. Catal., A*, 2005, **292**, 1; (*c*) X. Qi, M. R. Axet, K. Philippot, P. Lecante and P. Serp, *Dalton Trans.*, 2014, **43**, 9283.

16 D. Bouzouita, G. Lippens, E. A. Baquero, P. F. Fazzini, G. Pieters, Y. Coppel, P. Lecante, S. Tricard, L. M. Martínez-Prieto and B. Chaudret, *Nanoscale*, 2019, **11**, 16544.

17 C. Pan, F. Dassenoy, M.-J. Casanove, K. Philippot, C. Amiens, P. Lecante, A. Mosset and B. Chaudret, *J. Phys. Chem. B*, 1999, **103**, 10098.

18 S. Navalon, A. Dhakshinamoorthy, M. Alvaro and H. Garcia, *Coord. Chem. Rev.*, 2016, **312**, 99.

19 S. Stankovich, D. A. Dikin, R. D. Piner, K. A. Kohlhaas, A. Kleinhammes, Y. Jia, Y. Wu, S. T. Nguyen and R. S. Ruoff, *Carbon*, 2007, **45**, 1558.

20 L. Lai, L. Chen, D. Zhan, L. Sun, J. Liu, S. H. Lim, C. K. Poh, Z. Shen and J. Lin, *Carbon*, 2011, **49**, 3250.

21 D. J. Morgan, *Surf. Interface Anal.*, 2015, **47**, 1072.

22 F. Sen and G. Gökagaç, *J. Phys. Chem. C*, 2007, **111**, 5715.

23 P. W. N. M. van Leeuwen, *Homogeneous Catalysis—Understanding the Art*, Kluwer Academic Publishers, 2004.

504 | *Catal. Sci. Technol.*, 2021, **11**, 494–505

This journal is © The Royal Society of Chemistry 2021

24 See for example: (*a*) A. Denicourt-Nowicki, B. Leger and A. Roucoux, *Phys. Chem. Chem. Phys.*, 2011, **13**, 13510; (*b*) D. Duraczynska, A. Drelinkiewicz, E. Bielanska, E. M. Serwicka and L. Litynska-Dobrzynska, *Catal. Lett.*, 2011, **141**, 83.

25 See for example: (*a*) M. Fang and R. A. Sánchez-Delgado, *J. Catal.*, 2014, **311**, 357; (*b*) D. Formenti, C. Topf, K. Junge, F. Ragaini and M. Beller, *Catal.: Sci. Technol.*, 2016, **6**, 4473; (*c*) J. L. Fiorio, R. V. Gonçalves, E. Teixeira-Neto, M. A. Ortuño, N. López and L. M. Rossi, *ACS Catal.*, 2018, **8**, 3516.

26 R.-J. van Putten, J. C. van der Waal, E. de Jong, C. B. Rasrendra, H. J. Heeres and J. G. de Vries, *Chem. Rev.*, 2013, **113**, 1499.

27 T. Suoranta, M. Niemelä and P. Perämäki, *Talanta*, 2014, **119**, 425.

28 L. Lai, L. Chen, D. Zhan, L. Sun, J. Liu, S. H. Lim, C. K. Poh, Z. Shen and J. Lin, *Carbon*, 2011, **49**, 3250.

29 (*a*) W. S. Hummers and R. E. Offeman, *J. Am. Chem. Soc.*, 1958, **80**, 1339; (*b*) M. Feliz, M. Puche, P. Atienzar, P. Concepción, S. Cordier and Y. Molard, *ChemSusChem*, 2016, **9**, 1963.

This journal is © The Royal Society of Chemistry 2021

Catal. Sci. Technol., 2021, **11**, 494–505 | **505**